Acta Cryst E CRYSTALLOGRAPHIC COMMUNICATIONS

ISSN 2056-9890

Crystal structure, Hirshfeld surface analysis and interaction energy and DFT studies of (2*Z*)-4-benzyl-2-(2,4-dichlorobenzylidene)-2*H*-1,4-benzothiazin-3(4*H*)-one

Nada Kheira Sebbar,[a,b] Brahim Hni,[b] Tuncer Hökelek,[c] Mohamed Labd Taha,[a] Joel T. Mague,[d] Lhoussaine El Ghayati[b]* and El Mokhtar Essassi[b]

[a]Laboratoire de Chimie Appliquée et Environnement, Equipe de Chimie Bioorganique Appliquée, Faculté des Sciences, Université Ibn Zohr, Agadir, Morocco, [b]Laboratoire de Chimie Organique Hétérocyclique URAC 21, Pôle de Compétence Pharmacochimie, Av. Ibn Battouta, BP 1014, Faculté des Sciences, Université Mohammed V, Rabat, Morocco, [c]Department of Physics, Hacettepe University, 06800 Beytepe, Ankara, Turkey, and [d]Department of Chemistry, Tulane University, New Orleans, LA 70118, USA. *Correspondence e-mail: elghayatilhoussaine2018@gmail.com

Received 24 September 2019
Accepted 4 October 2019

Edited by A. J. Lough, University of Toronto, Canada

Keywords: crystal structure; dihydrothiazine; hydrogen bond; π-stacking; Hirshfeld surface.

CCDC reference: 1957875

Supporting information: this article has supporting information at journals.iucr.org/e

The title compound, $C_{22}H_{15}Cl_2NOS$, contains 1,4-benzothiazine and 2,4-dichlorobenzylidene units, where the dihydrothiazine ring adopts a screw-boat conformation. In the crystal, intermolecular $C-H_{Bnz}\cdots O_{Thz}$ (Bnz = benzene and Thz = thiazine) hydrogen bonds form corrugated chains extending along the *b*-axis direction which are connected into layers parallel to the *bc* plane by intermolecular $C-H_{Methy}\cdots S_{Thz}$ (Methy = methylene) hydrogen bonds, enclosing $R_4^4(22)$ ring motifs. Offset π-stacking interactions between 2,4-dichlorophenyl rings [centroid–centroid = 3.7701 (8) Å] and π-interactions which are associated by $C-H_{Bnz}\cdots\pi$(ring) and $C-H_{Dchlphy}\cdots\pi$(ring) (Dchlphy = 2,4-dichlorophenyl) interactions may be effective in the stabilization of the crystal structure. The Hirshfeld surface analysis of the crystal structure indicates that the most important contributions for the crystal packing are from H···H (29.1%), H···C/C···H (27.5%), H···Cl/Cl···H (20.6%) and O···H/H···O (7.0%) interactions. Hydrogen-bonding and van der Waals interactions are the dominant interactions in the crystal packing. Computational chemistry indicates that in the crystal, the $C-H_{Bnz}\cdots O_{Thz}$ and $C-H_{Methy}\cdots S_{Thz}$ hydrogen-bond energies are 55.0 and 27.1 kJ mol^{-1}, respectively. Density functional theory (DFT) optimized structures at the B3LYP/6-311G(d,p) level are compared with the experimentally determined molecular structure in the solid state. The HOMO–LUMO behaviour was elucidated to determine the energy gap.

1. Chemical context

1,4-Benzothiazine derivatives constitute an important class of heterocyclic systems. These molecules exhibit a wide range of biological applications, indicating the fact that the 1,4-benzothiazine moiety is a template potentially useful in medicinal chemistry research and therapeutic applications, such as the anti-inflammatory (Trapani *et al.*, 1985; Gowda *et al.*, 2011), antipyretic (Warren & Knaus, 1987), antimicrobial (Armenise *et al.*, 2012; Rathore & Kumar, 2006), antiviral (Malagu *et al.*, 1998), anticancer (Gupta *et al.*, 1985; Gupta & Gupta, 1991) and anti-oxidant (Zia-ur-Rehman *et al.*, 2009) areas. They have also been reported as precursors for the syntheses of new compounds (Sebbar *et al.*, 2015*a*; Vidal *et al.*, 2006) possessing antidiabetic (Tawada *et al.*, 1990) and anticorrosion activities (Ellouz *et al.*, 2016*a*,*b*; Sebbar *et al.*, 2016*a*). They also possess biological properties (Hni *et al.*, 2019*a*,*b*; Sebbar *et al.*, 2017; Ellouz *et al.*, 2017*a*,*b*, 2018). As a continuation of our research on the development of *N*-substituted 1,4-benzothiazine deri-

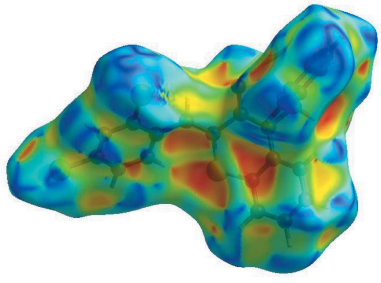

vatives and the evaluation of their potential pharmacological activities, we report here the synthesis of (2*Z*)-4-benzyl-2-(2,4-dichlorobenzylidene)-2*H*-1,4-benzothiazin-3(4*H*)-one, (I), by the reaction of benzyl chloride with (*Z*)-2-(2,4-dichlorobenzylidene)-2*H*-1,4-benzothiazin-3(4*H*)-one and potassium carbonate in the presence of tetra-*n*-butylammonium bromide (as catalyst). The molecular and crystal structures, together with the Hirshfeld surface analysis, the intermolecular interaction energies and density functional theory (DFT) computational calculations were carried out at the B3LYP/6-311G(d,p) and B3LYP/6-311G(d,p) levels, respectively, for (I) (see Scheme 1).

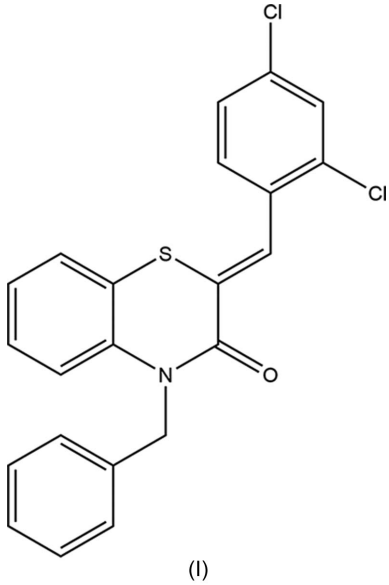

(I)

Scheme 1

2. Structural commentary

The title compound, (I), contains 1,4-benzothiazine and 2,4-dichlorobenzylidene units (Fig. 1), where the dihydrothiazine ring, *B* (atoms S1/N1/C1/C6–C8), adopts a screw-boat conformation with puckering parameters (Cremer & Pople, 1975) of Q_T = 0.4331 (10) Å, θ = 68.34 (16)° and φ = 333.95 (17)°. The planar rings *A* (C1–C6), *C* (C10–C15) and *D* (C17–C22) are oriented at dihedral angles of *A*/*C* = 60.49 (4)°, *A*/*D* = 79.69 (4)° and *C*/*D* = 41.29 (4)°. Atoms Cl1 and Cl2 are −0.0156 (3) and 0.0499 (4) Å from ring *C* and so are almost coplanar.

Table 1
Hydrogen-bond geometry (Å, °).

*Cg*1 and *Cg*4 are the centroids of rings *A* (C1–C6) and *D* (C17–C22), respectively.

D—H···*A*	*D*—H	H···*A*	*D*···*A*	*D*—H···*A*
C4—H4···O1^{ix}	0.936 (19)	2.51 (2)	3.3346 (17)	147.7 (15)
C16—H16*B*···S1^{v}	0.945 (16)	2.852 (16)	3.7011 (13)	149.9 (12)
C3—H3···*Cg*4^{ix}	0.938 (17)	2.901 (17)	3.6428 (15)	136.8 (13)
C14—H14···*Cg*4^{x}	0.971 (19)	2.710 (18)	3.5593 (15)	146.8 (14)
C18—H18···*Cg*1^{xi}	0.979 (18)	2.969 (18)	3.6759 (16)	130.0 (13)

Symmetry codes: (v) $x, -y+\frac{1}{2}, z-\frac{1}{2}$; (ix) $-x+1, y-\frac{1}{2}, -z+\frac{1}{2}$; (x) $x-1, -y-\frac{1}{2}, z-\frac{1}{2}$; (xi) $x, -y-\frac{1}{2}, z-\frac{3}{2}$.

3. Supramolecular features

In the crystal, intermolecular C—H_{Bnz}···O_{Thz} (Bnz = benzene and Thz = thiazine) hydrogen bonds form corrugated chains extending along the *b*-axis direction which are connected into layers parallel to the *bc* plane by intermolecular C—H_{Methy}···S_{Thz} (Methy = methylene) hydrogen bonds, enclosing $R_4^4(22)$ ring motifs (Bernstein *et al.*, 1995) (Table 1 and Fig. 2). Offset π-stacking interactions between 2,4-dichlorophenyl rings *C* [atoms C10–C15; *Cg*3···*Cg*3^{i}, where *Cg*3 is the centroid of ring *C*; symmetry code: (i) $-x, -y+1, -z+1$], may further stabilize the structure, with a centroid–centroid distance of 3.7701 (8) Å, together with π-interactions, *i.e.* C—H_{Bnz}···π(ring) and C—$H_{Dchlphy}$···π(ring) (Dchlphy = 2,4-dichlorophenyl). The Hirshfeld surface analysis of the crystal

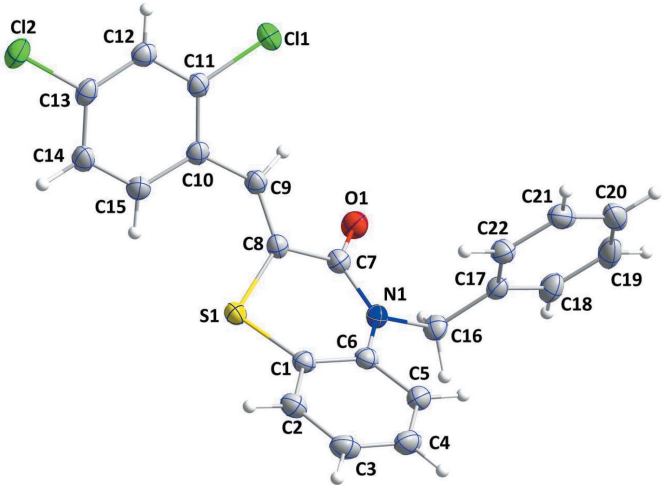

Figure 1
The molecular structure of the title compound with the atom-numbering scheme. Displacement ellipsoids are drawn at the 50% probability level.

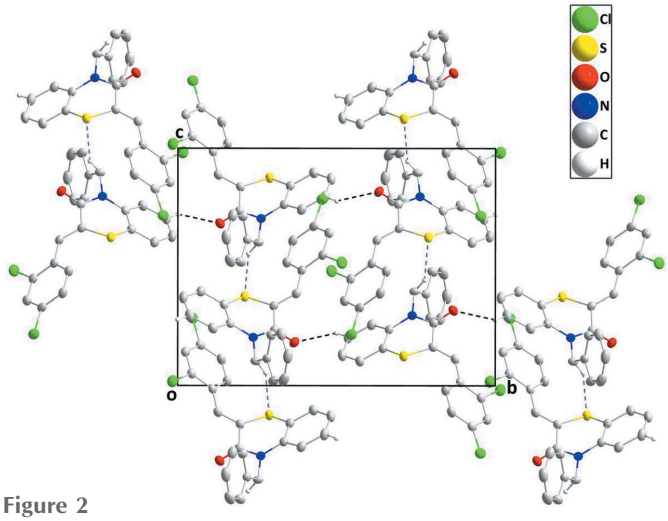

Figure 2
A partial packing diagram, viewed along the *a*-axis direction, with C—H_{Bnz}···O_{Thz} and C—H_{Methy}···S_{Thz} (Bnz = benzene, Thz = thiazine and Methy = methylene) hydrogen bonds shown, respectively, as black and light-purple dashed lines.

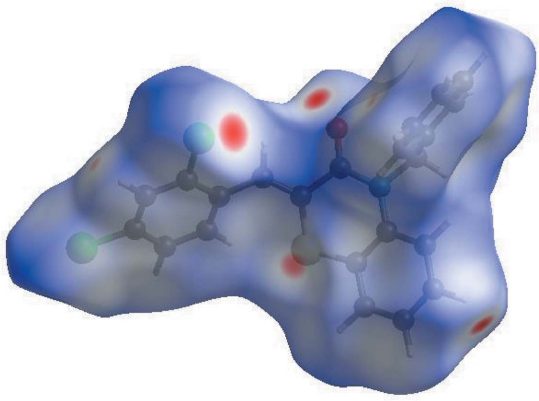

Figure 3
View of the 3D Hirshfeld surface of the title compound, plotted over d_{norm} in the range −0.1634 to 1.5051 a.u.

structure indicates that the most important contributions for the crystal packing are from H···H (29.1%), H···C/C···H (27.5%), H···Cl/Cl···H (20.6%) and O···H/H···O (7.0%) interactions. Hydrogen-bonding and van der Waals interactions are the dominant interactions in the crystal packing.

4. Hirshfeld surface analysis

In order to visualize the intermolecular interactions in the crystal of (I), a Hirshfeld surface (HS) analysis (Hirshfeld, 1977; Spackman & Jayatilaka, 2009) was carried out using *CrystalExplorer* (Version 17.5; Turner *et al.*, 2017). In the HS plotted over d_{norm} (Fig. 3), the white surface indicates contacts with distances equal to the sum of the van der Waals radii, and the red and blue colours indicate distances shorter (in close contact) or longer (distinct contact) than the van der Waals radii, respectively (Venkatesan *et al.*, 2016). The bright-red spots appearing near atoms O1, S1 and H4 indicate their roles as the respective donors and/or acceptors; they also appear as blue and red regions corresponding to positive and negative potentials on the HS mapped over electrostatic potential (Spackman *et al.*, 2008; Jayatilaka *et al.*, 2005), as shown in Fig. 4. The blue regions indicate the positive electrostatic potential (hydrogen-bond donors), while the red regions indicate the negative electrostatic potential (hydrogen-bond acceptors). The shape-index of the HS is a tool to visualize the π–π stacking by the presence of adjacent red and blue triangles; if there are no adjacent red and/or blue triangles, then there are no π–π interactions. Fig. 5 clearly suggest that there are π–π interactions in (I). The overall two-dimensional (2D) fingerprint plot (Fig. 6*a*) and those delineated into H···H, H···C/C···H, H···Cl/Cl···H, O···H/H···O, C···C, S···H/H···S and Cl···C/C···Cl contacts (McKinnon *et al.*, 2007) are illustrated in Figs. 6(*b*)–(*h*), respectively, together with their

Table 2
Selected interatomic distances (Å).

Cl1···Cl1^{i}	3.2439 (5)	C6···C22	3.4830 (18)
Cl1···C14^{ii}	3.4981 (14)	C6···C12^{v}	3.5828 (18)
Cl1···H9	2.647 (16)	C7···C22	3.4391 (18)
Cl2···H19^{iii}	2.96 (2)	C10···C12^{ii}	3.4871 (18)
Cl2···H9^{ii}	3.044 (16)	C14···C20^{iv}	3.572 (2)
Cl2···H4^{iv}	3.138 (18)	C5···H16*A*	2.563 (16)
S1···Cl2^{v}	3.5832 (5)	C6···H22	2.904 (15)
S1···Cl2^{v}	3.5832 (5)	C8···H15	2.929 (18)
S1···N1	3.0801 (11)	C16···H5	2.556 (18)
S1···C15	3.1625 (14)	C17···H5	2.829 (18)
S1···C13^{v}	3.6033 (13)	C18···H3^{vi}	2.998 (17)
S1···H15	2.578 (18)	C21···H12^{i}	2.845 (18)
O1···C17	3.2096 (16)	H14···C20^{iv}	2.964 (18)
O1···C4^{vi}	3.3346 (17)	H14···C21^{iv}	2.899 (18)
O1···H9	2.406 (16)	H14···C22^{iv}	2.990 (18)
O1···H16*B*	2.345 (16)	H15···C19^{iv}	2.951 (18)
O1···H4^{vi}	2.51 (2)	H16*B*···S1^{v}	2.852 (16)
N1···S1	3.0801 (11)	H16*B*···C1^{v}	2.973 (16)
N1···H22	2.552 (15)	H18···C6^{v}	2.934 (19)
C1···C12^{v}	3.4639 (18)	H5···H16*A*	2.16 (2)
C1···C13^{v}	3.4372 (18)	H12···H21^{i}	2.46 (3)
C2···C12^{v}	3.541 (2)	H15···H21^{viii}	2.51 (3)
C3···C3^{vii}	3.485 (2)	H16*B*···H18	2.51 (2)
C5···C22	3.4988 (19)	H18···H22^{v}	2.53 (2)
C5···C17	3.4201 (18)		

Symmetry codes: (i) $-x+1, -y+1, -z+1$; (ii) $-x, -y+1, -z+1$; (iii) $x-1, y, z+1$; (iv) $x-1, -y+\frac{1}{2}, z+\frac{1}{2}$; (v) $x, -y+\frac{1}{2}, z-\frac{1}{2}$; (vi) $-x+1, y+\frac{1}{2}, -z+\frac{1}{2}$; (vii) $-x+1, -y, -z+1$; (viii) $x-1, y, z$.

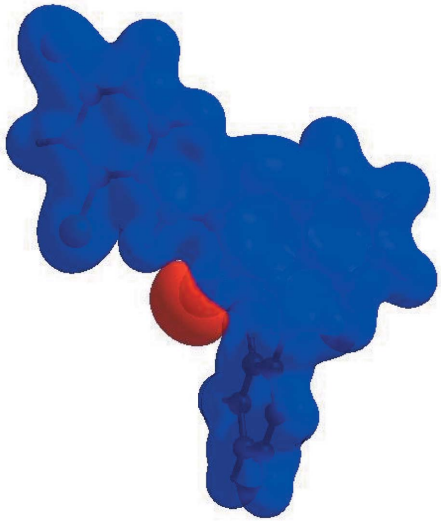

Figure 4
View of the 3D Hirshfeld surface of the title compound, plotted over electrostatic potential energy in the range −0.0500 to 0.0500 a.u., using the STO-3G basis set at the Hartree–Fock level of theory. Hydrogen-bond donors and acceptors are shown as blue and red regions around the atoms corresponding to positive and negative potentials, respectively.

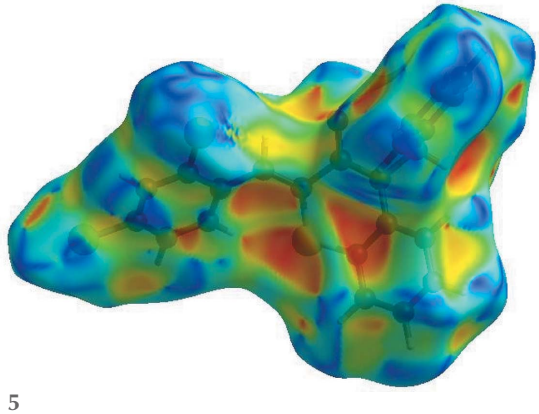

Figure 5
Hirshfeld surface of the title compound plotted over shape-index.

relative contributions to the Hirshfeld surface. The most important interaction is H···H, contributing 29.1% to the overall crystal packing, which is reflected in Fig. 6(*b*) as widely scattered points of high density due to the large hydrogen content of the molecule with the tip at $d_e = d_i = 1.17$ Å, due to the short interatomic H···H contacts (Table 2). In the presence of C—H···π interactions, the pairs of characteristic wings resulting in the fingerprint plot delineated into H···C/C···H contacts (Fig. 6*c*), with a 27.5% contribution to the HS, arises from the H···C/C···H contacts (Table 2) and are viewed as pairs of spikes with the tips at $d_e + d_i = 2.82$ and 2.78 Å for thin and thick spikes, respectively. The pair of scattered points of the wings resulting in the fingerprint plots delineated into H···Cl/Cl···H (Fig. 6*d*), with a 20.6% contribution to the HS, has a symmetrical distribution of points with the edges at $d_e + d_i = 2.78$ Å arising from the H···Cl/Cl···H contacts (Table 2). The pair of characteristic wings resulting in the fingerprint plot delineated into O···H/H···O contacts (Fig. 6*e*), with a 7.0% contribution to the HS, arises from the O···H/H···O contacts (Table 2) and is viewed as a pair of spikes with the tips at $d_e + d_i = 2.35$ Å. The C···C contacts (Fig. 6*f*) have an arrow-shaped distribution of points with the tip at $d_e = d_i = 1.7$ Å. Finally, the characteristic wings resulting in the fingerprint plots delineated into S···H/H···S and Cl···C/C···Cl contacts (Figs. 6*g* and 6*h*), with 4.0 and 2.2% contributions to the HS, arise from the S···H/H···S and Cl···C/C···Cl contacts (Table 2) and are viewed with the tips at $d_e = d_i = 2.70$ Å and $d_e + d_i = 3.46$ Å, respectively.

The Hirshfeld surface representations with the function d_{norm} plotted onto the surface are shown for the H···H, H···C/C···H, H···Cl/Cl···H, O···H/H···O, C···C and S···H/H···S interactions in Figs. 7(*a*)–(*f*), respectively.

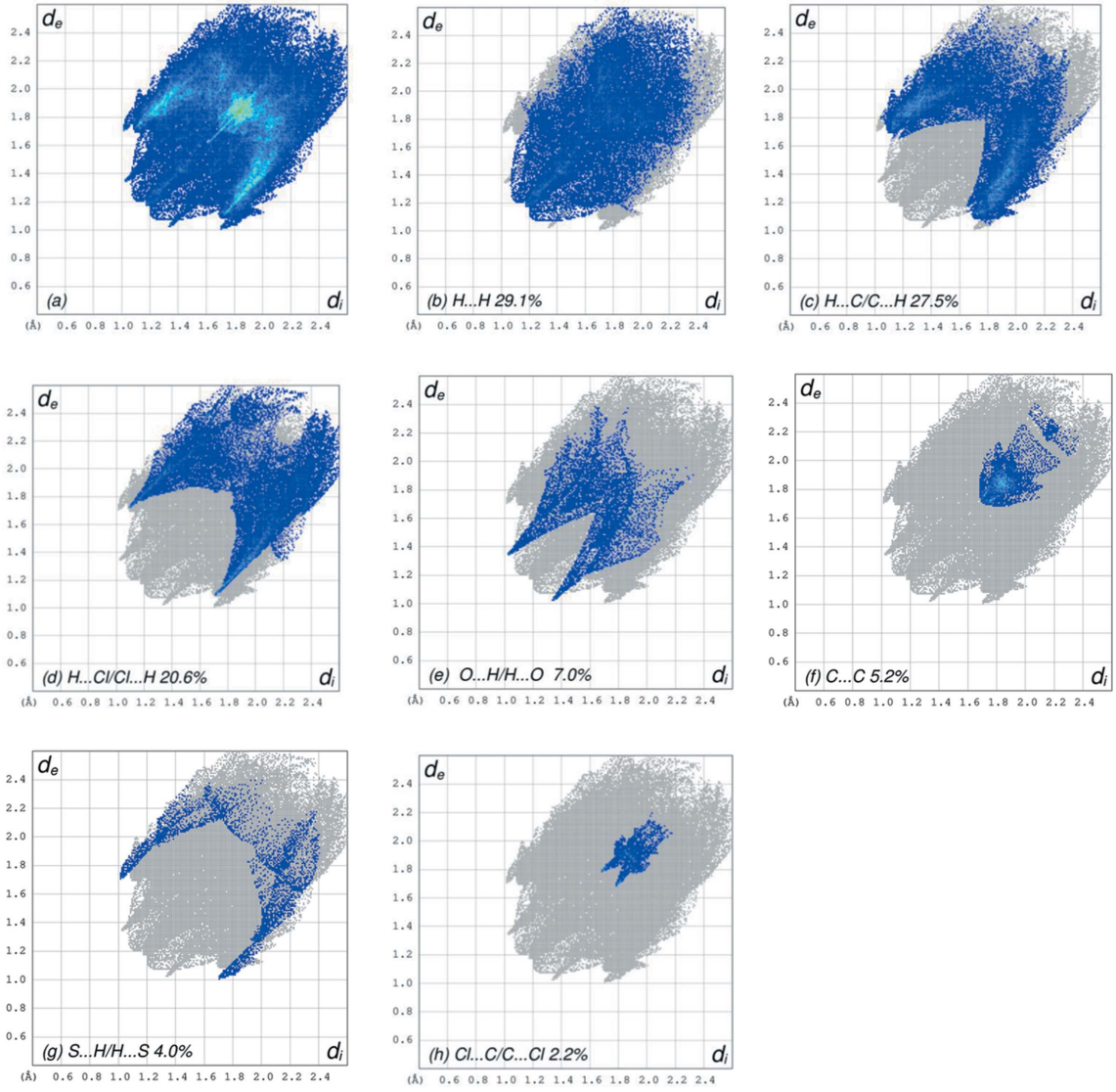

Figure 6
The full 2D fingerprint plots for the title compound, showing (*a*) all interactions, and delineated into (*b*) H···H, (*c*) H···C/C···H, (*d*) H···Cl/Cl···H, (*e*) O···H/H···O, (*f*) C···C, (*g*) S···H/H···S and (*h*) Cl···C/C···Cl interactions. The d_i and d_e values are the closest internal and external distances (in Å) from given points on the Hirshfeld surface contacts.

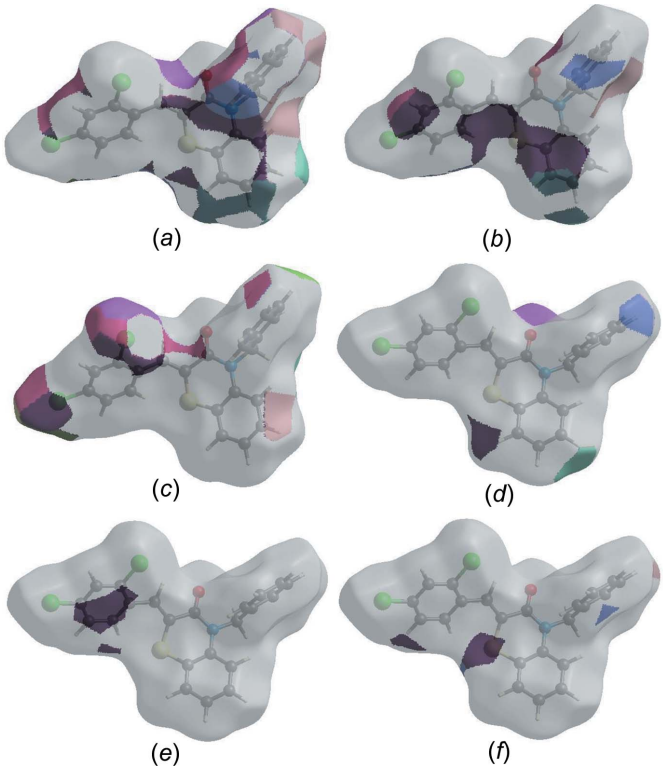

Figure 7
The Hirshfeld surface representations with the function d_{norm} plotted onto the surface for (*a*) H···H, (*b*) H···C/C···H, (*c*) H···Cl/Cl···H, (*d*) O···H/H···O, (*e*) C···C and (*f*) S···H/H···S interactions.

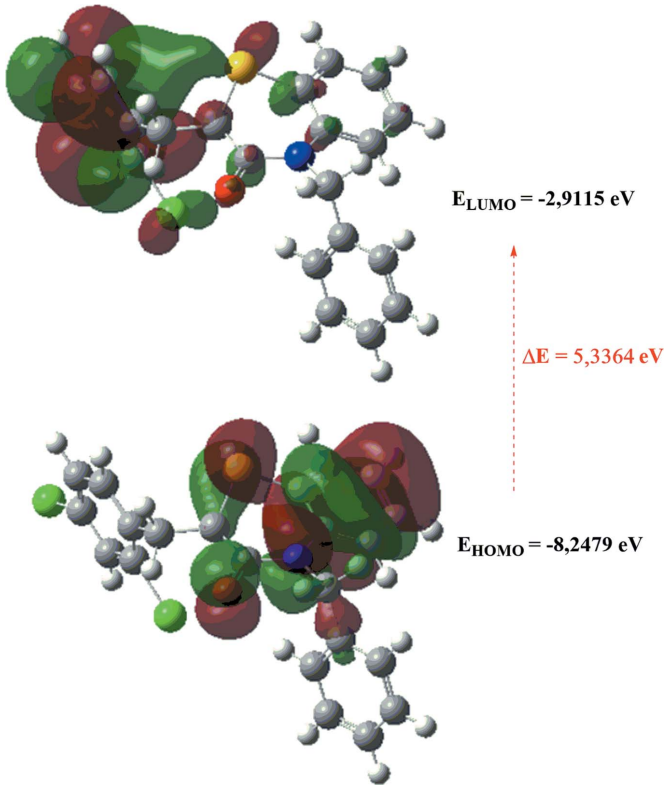

Figure 8
The energy band gap of the title compound.

Table 3
Comparison of the selected (X-ray and DFT) geometric data (Å, °).

Bonds/angles	X-ray	B3LYP/6–311G(d,p)
Cl1—C11	1.7357 (13)	1.80981
Cl2—C13	1.7382 (13)	1.80489
S1—C8	1.7525 (12)	1.80120
S1—C1	1.7561 (13)	1.82629
O1—C7	1.2228 (16)	1.23968
N1—C7	1.3759 (16)	1.38157
N1—C6	1.4192 (16)	1.41776
N1—C16	1.4661 (16)	1.47048
C8—S1—C1	100.14 (6)	98.69028
C7—N1—C6	125.51 (10)	124.58623
C7—N1—C16	115.14 (10)	116.12685
C6—N1—C16	119.20 (10)	119.26679
C2—C1—C6	120.71 (12)	121.24260
C2—C1—S1	117.26 (10)	117.48822
C6—C1—S1	122.02 (10)	121.26667

The Hirshfeld surface analysis confirms the importance of H-atom contacts in establishing the packing. The large number of H···H, H···C/C···H, H···Cl/Cl···H and O···H/H···O interactions suggest that van der Waals interactions and hydrogen bonding play the biggest roles in the crystal packing (Hathwar *et al.*, 2015).

5. Interaction energy calculations

The intermolecular interaction energies are calculated using CE–B3LYP/6-31G(d,p) energy model available in *Crystal-Explorer* (CE) (Version 17.5; Turner *et al.*, 2017), where a cluster of molecules would need to be generated by applying crystallographic symmetry operations with respect to a selected central molecule within a default radius of 3.8 Å (Turner *et al.*, 2014). The total intermolecular energy (E_{tot}) is the sum of the electrostatic (E_{ele}), polarization (E_{pol}), dispersion (E_{dis}) and exchange-repulsion (E_{rep}) energies (Turner *et al.*, 2015), with scale factors of 1.057, 0.740, 0.871 and 0.618, respectively (Mackenzie *et al.*, 2017). Hydrogen-bonding interaction energies (in kJ mol^{-1}) were calculated as −20.3 (E_{ele}), −2.6 (E_{pol}), −79.4 (E_{dis}), 60.7 (E_{rep}) and −55.0 (E_{tot}) for C—H_{Bnz}···O_{Thz} hydrogen-bonding interactions, and −5.8 (E_{ele}), −1.0 (E_{pol}), −51.0 (E_{dis}), 39.3 (E_{rep}) and −27.1 (E_{tot}) for C—H_{Methy}···S_{Thz} hydrogen-bonding interactions.

6. DFT calculations

The optimized structure of (I) in the gas phase was generated theoretically *via* density functional theory (DFT) using standard B3LYP functional and 6-311G(d,p) basis-set calculations (Becke, 1993), as implemented in *GAUSSIAN09* (Frisch *et al.*, 2009). The theoretical and experimental results were in good agreement (Table 3). The highest-occupied molecular orbital (HOMO), acting as an electron donor, and the lowest-unoccupied molecular orbital (LUMO), acting as an electron acceptor, are very important parameters for quantum chemistry. When the energy gap is small, the molecule is highly polarizable and has high chemical reactivity. The DFT calculations provide some important information on the reactivity

Table 4
Calculated energies..

Molecular Energy (a.u.) (eV)	Compound (I)
Total Energy *TE* (eV)	−62249, 6662
E_{HOMO} (eV)	−8.2479
E_{LUMO} (eV)	−2.9115
Gap ΔE (eV)	5.3364
Dipole moment, μ (Debye)	3.4723
Ionization potential, I (eV)	8.2479
Electron affinity, A	2.9115
Electro negativity, χ	5.3364
Hardness, η	2.6682
Electrophilicity index, ω	5.8340
Softness, σ	0.3748
Fraction of electron transferred, ΔN	0.2662

and site selectivity of the molecular framework. E_{HOMO} and E_{LUMO} clarifying the inevitable charge exchange collaboration inside the studied material, electronegativity (χ), hardness (η), potential (μ), electrophilicity (ω) and softness (σ) are recorded in Table 4. The significance of η and σ is to evaluate both the reactivity and stability. The electron transition from the HOMO to the LUMO energy level is shown in Fig. 8. The HOMO and LUMO are localized in the plane extending from the whole molecule. The energy band gap ($\Delta E = E_{LUMO} - E_{HOMO}$) of the molecule was about 5.3364 eV, and the frontier molecular orbital (FMO) energies, E_{HOMO} and E_{LUMO}, were −8.2479 and −2.9115 eV, respectively.

Table 5
Experimental details.

Crystal data	
Chemical formula	$C_{22}H_{15}Cl_2NOS$
M_r	412.31
Crystal system, space group	Monoclinic, $P2_1/c$
Temperature (K)	150
a, b, c (Å)	9.0373 (7), 16.6798 (13), 12.511 (1)
β (°)	95.982 (2)
V (Å^3)	1875.6 (3)
Z	4
Radiation type	Cu $K\alpha$
μ (mm^{-1})	4.25
Crystal size (mm)	0.15 × 0.13 × 0.09
Data collection	
Diffractometer	Bruker D8 VENTURE PHOTON 100 CMOS
Absorption correction	Numerical (*SADABS*; Krause *et al.*, 2015)
T_{min}, T_{max}	0.59, 0.70
No. of measured, independent and observed [$I > 2\sigma(I)$] reflections	48886, 3847, 3650
R_{int}	0.038
(sin $\theta/\lambda)_{max}$ (Å^{-1})	0.625
Refinement	
$R[F^2 > 2\sigma(F^2)]$, $wR(F^2)$, S	0.026, 0.070, 1.05
No. of reflections	3847
No. of parameters	304
H-atom treatment	All H-atom parameters refined
$\Delta\rho_{max}$, $\Delta\rho_{min}$ (e Å^{-3})	0.22, −0.26

Computer programs: *APEX3* (Bruker, 2016), *SAINT* (Bruker, 2016), *SHELXT* (Sheldrick, 2015*a*), *SHELXL2018* (Sheldrick, 2015*b*), *DIAMOND* (Brandenburg & Putz, 2012) and *SHELXTL* (Bruker, 2016).

7. Database survey

A search in the Cambridge Structural Database (Groom *et al.*, 2016; updated to June 2019) for compounds containing the fragment II (with R_1 = Ph and R_2 = C; see Scheme 2) gave 14 hits. With R_1 = Ph and R_2 = $CH_2C{\equiv}CH$ (**IIa**) (Sebbar *et al.*, 2014*a*), CH_2COOH (**IIb**) (Sebbar *et al.*, 2016*c*), 2-(2-oxo-1,3-oxazolidin-3-yl)ethyl (**IIc**) (Sebbar *et al.*, 2016*b*) and (3-phenyl-4,5-dihydro-1,2-oxazol-5-yl)methyl (**IIf**) (Sebbar *et al.*, 2015*b*)] (Scheme 2), there are other examples with R_1 = 4-FC_6H_4 and R_2 = $CH_2C{\equiv}CH$ (**IIa**) (Hni *et al.*, 2019*a*), R_1 = 4-ClC_6H_4 and R_2 = CH_2Ph2 (**IId**) (Ellouz *et al.*, 2016*c*), and R_1 = 2-ClC_6H_4 and R_2 = $CH_2C{\equiv}CH$ (**IIa**) (Sebbar *et al.*, 2017) (Scheme 2). In all compounds, the configuration about the benzylidene-group $C{=}CHC_6H_5$ bond is *Z*, and in the majority of these, the heterocyclic ring is quite nonplanar, with the dihedral angle between the plane defined by the benzene ring plus the N and S atoms, and that defined by the N and S atoms and the other two C atoms separating them ranging from *ca* 29 (for **IIa**) to 36° (for **IIf**). The other two (**IIa** and **IIc**) have the benzothiazine unit nearly planar, with corresponding dihedral angles of *ca* 3–4°.

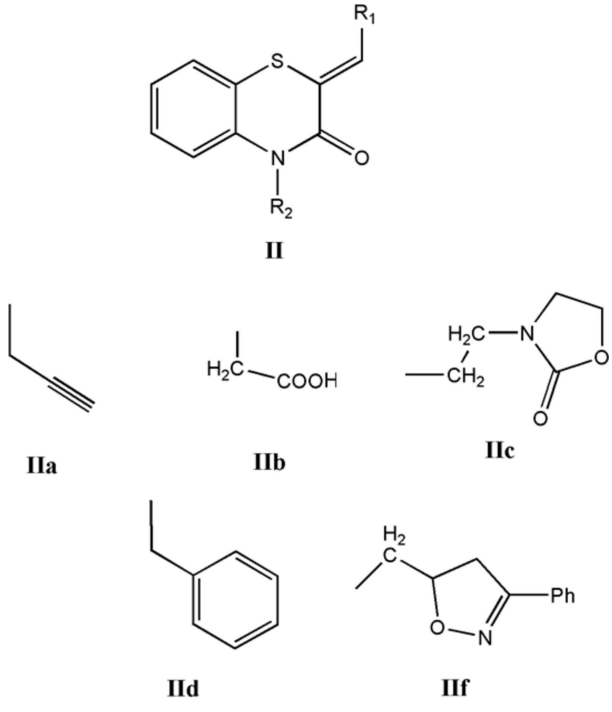

Scheme 2

8. Synthesis and crystallization

To a solution of (*Z*)-2-(2,4-dichlorobenzylidene)-2*H*-1,4-benzothiazin-3(4*H*)-one (3.21 mmol), benzyl chloride (6.52 mmol) and potassium carbonate (6.51 mmol) in dimethylformamide (DMF; 17 ml) was added a catalytic amount of tetra-*n*-butylammonium bromide (0.33 mmol). The mixture was stirred for 24 h. The solid material was removed by filtration and the solvent evaporated under vacuum. The solid product was purified by recrystallization from ethanol to afford colourless crystals in 82% yield.

9. Refinement

The experimental details, including the crystal data, data collection and refinement, are summarized in Table 5. H atoms were located in a difference Fourier map and refined freely.

Acknowledgements

The support of NSF-MRI for the purchase of the diffractometer and Tulane University for support of the Tulane Crystallography Laboratory are gratefully acknowledged.

Funding information

Funding for this research was provided by: NSF-MRI (grant No. 1228232); Hacettepe University Scientific Research Project Unit (grant No. 013 D04 602 004 to TH).

References

Armenise, D., Muraglia, M., Florio, M. A., Laurentis, N. D., Rosato, A., Carrieri, A., Corbo, F. & Franchini, C. (2012). *Mol. Pharmacol.* **50**, 1178–1188.

Becke, A. D. (1993). *J. Chem. Phys.* **98**, 5648–5652.

Bernstein, J., Davis, R. E., Shimoni, L. & Chang, N. L. (1995). *Angew. Chem. Int. Ed. Engl.* **34**, 1555–1573.

Brandenburg, K. & Putz, H. (2012). *DIAMOND*. Crystal Impact GbR, Bonn, Germany.

Bruker (2016). *APEX3*, *SAINT*, *SADABS* and *SHELXTL*. Bruker AXS Inc., Madison, Wisconsin, USA.

Cremer, D. & Pople, J. A. (1975). *J. Am. Chem. Soc.* **97**, 1354–1358.

Ellouz, M., Elmsellem, H., Sebbar, N. K., Steli, H., Al Mamari, K., Nadeem, A., Ouzidan, Y., Essassi, E. M., Abdel-Rahaman, I. & Hristov, P. (2016*b*). *J. Mater. Environ. Sci.* **7**, 2482–2497.

Ellouz, M., Sebbar, N. K., Boulhaoua, M., Essassi, E. M. & Mague, J. T. (2017*a*). *IUCrData*, **2**, x170646.

Ellouz, M., Sebbar, N. K., Elmsellem, H., Steli, H., Fichtali, I., Mohamed, A. M. M., Mamari, K. A., Essassi, E. M. & Abdel-Rahaman, I. (2016*a*). *J. Mater. Environ. Sci.* **7**, 2806–2819.

Ellouz, M., Sebbar, N. K., Essassi, E. M., Ouzidan, Y., Mague, J. T. & Zouihri, H. (2016*c*). *IUCrData*, **1**, x160764.

Ellouz, M., Sebbar, N. K., Fichtali, I., Ouzidan, Y., Mennane, Z., Charof, R., Mague, J. T., Urrutigoïty, M. & Essassi, E. M. (2018). *Chem. Cent. J.* **12**, 123.

Ellouz, M., Sebbar, N. K., Ouzidan, Y., Essassi, E. M. & Mague, J. T. (2017*b*). *IUCrData*, **2**, x170097.

Frisch, M. J., *et al.* (2009). *GAUSSIAN09*. Gaussian Inc., Wallingford, CT, USA.

Gowda, J., Khader, A. M. A., Kalluraya, B., Shree, P. & Shabaraya, A. R. (2011). *Eur. J. Med. Chem.* **46**, 4100–4106.

Groom, C. R., Bruno, I. J., Lightfoot, M. P. & Ward, S. C. (2016). *Acta Cryst.* B**72**, 171–179.

Gupta, R. R., Kumar, R. & Gautam, R. K. (1985). *J. Fluor. Chem.* **28**, 381–385.

Gupta, V. & Gupta, R. R. (1991). *J. Prakt. Chem.* **333**, 153–156.

Hathwar, V. R., Sist, M., Jørgensen, M. R. V., Mamakhel, A. H., Wang, X., Hoffmann, C. M., Sugimoto, K., Overgaard, J. & Iversen, B. B. (2015). *IUCrJ*, **2**, 563–574.

Hirshfeld, H. L. (1977). *Theor. Chim. Acta*, **44**, 129–138.

Hni, B., Sebbar, N. K., Hökelek, T., El Ghayati, L., Bouzian, Y., Mague, J. T. & Essassi, E. M. (2019*b*). *Acta Cryst.* E**75**, 593–599.

Hni, B., Sebbar, N. K., Hökelek, T., Ouzidan, Y., Moussaif, A., Mague, J. T. & Essassi, E. M. (2019*a*). *Acta Cryst.* E**75**, 372–377.

Jayatilaka, D., Grimwood, D. J., Lee, A., Lemay, A., Russel, A. J., Taylor, C., Wolff, S. K., Cassam-Chenai, P. & Whitton, A. (2005). *TONTO - A System for Computational Chemistry*. Available at: http://hirshfeldsurface.net/.

Krause, L., Herbst-Irmer, R., Sheldrick, G. M. & Stalke, D. (2015). *J. Appl. Cryst.* **48**, 3–10.

Mackenzie, C. F., Spackman, P. R., Jayatilaka, D. & Spackman, M. A. (2017). *IUCrJ*, **4**, 575–587.

Malagu, K., Boustie, J., David, M., Sauleau, J., Amoros, M., Girre, R. L. & Sauleau, A. (1998). *Pharm. Pharmacol. Commun.* **4**, 57–60.

McKinnon, J. J., Jayatilaka, D. & Spackman, M. A. (2007). *Chem. Commun.* pp. 3814–3816.

Rathore, B. S. & Kumar, M. (2006). *Bioorg. Med. Chem.* **14**, 5678–5682.

Sebbar, N. K., Ellouz, M., Essassi, E. M., Ouzidan, Y. & Mague, J. T. (2015*a*). *Acta Cryst.* E**71**, o999.

Sebbar, N. K., Ellouz, M., Essassi, E. M., Saadi, M. & El Ammari, L. (2015*b*). *Acta Cryst.* E**71**, o423–o424.

Sebbar, N. K., Ellouz, M., Essassi, E. M., Saadi, M. & El Ammari, L. (2016*a*). *IUCrData*, **1**, x161012.

Sebbar, N. K., Ellouz, M., Mague, J. T., Ouzidan, Y., Essassi, E. M. & Zouihri, H. (2016*c*). *IUCrData*, **1**, x160863.

Sebbar, N. K., Ellouz, M., Ouzidan, Y., Kaur, M., Essassi, E. M. & Jasinski, J. P. (2017). *IUCrData*, **2**, x170889.

Sebbar, N. K., Mekhzoum, M. E. M., Essassi, E. M., Zerzouf, A., Talbaoui, A., Bakri, Y., Saadi, M. & Ammari, L. E. (2016*b*). *Res. Chem. Intermed.* **42**, 6845–6862.

Sebbar, N. K., Zerzouf, A., Essassi, E. M., Saadi, M. & El Ammari, L. (2014*a*). *Acta Cryst.* E**70**, o614.

Sheldrick, G. M. (2015*a*). *Acta Cryst.* A**71**, 3–8.

Sheldrick, G. M. (2015*b*). *Acta Cryst.* C**71**, 3–8.

Spackman, M. A. & Jayatilaka, D. (2009). *CrystEngComm*, **11**, 19–32.

Spackman, M. A., McKinnon, J. J. & Jayatilaka, D. (2008). *CrystEngComm*, **10**, 377–388.

Tawada, H., Sugiyama, Y., Ikeda, H., Yamamoto, Y. & Meguro, K. (1990). *Chem. Pharm. Bull.* **38**, 1238–1245.

Trapani, G., Reho, A., Morlacchi, F., Latrofa, A., Marchini, P., Venturi, F. & Cantalamessa, F. (1985). *Farmaco Ed. Sci.* **40**, 369–376.

Turner, M. J., Grabowsky, S., Jayatilaka, D. & Spackman, M. A. (2014). *J. Phys. Chem. Lett.* **5**, 4249–4255.

Turner, M. J., McKinnon, J. J., Wolff, S. K., Grimwood, D. J., Spackman, P. R., Jayatilaka, D. & Spackman, M. A. (2017). *CrystalExplorer17*. University of Western Australia.

Turner, M. J., Thomas, S. P., Shi, M. W., Jayatilaka, D. & Spackman, M. A. (2015). *Chem. Commun.* **51**, 3735–3738.

Venkatesan, P., Thamotharan, S., Ilangovan, A., Liang, H. & Sundius, T. (2016). *Spectrochim. Acta A Mol. Biomol. Spectrosc.* **153**, 625–636.

Vidal, A., Madelmont, J. C. & Mounetou, E. A. (2006). *Synthesis*, **2006**, 591–593.

Warren, B. K. & Knaus, E. E. (1987). *Eur. J. Med. Chem.* **22**, 411–415.

Zia-ur-Rehman, M., Choudary, J. A., Elsegood, M. R. J., Siddiqui, H. L. & Khan, K. M. (2009). *Eur. J. Med. Chem.* **44**, 1311–1316.

supporting information

Acta Cryst. (2019). E**75**, 1650-1656 [https://doi.org/10.1107/S2056989019013586]

Crystal structure, Hirshfeld surface analysis and interaction energy and DFT studies of (2*Z*)-4-benzyl-2-(2,4-dichlorobenzylidene)-2*H*-1,4-benzothiazin-3(4*H*)-one

Nada Kheira Sebbar, Brahim Hni, Tuncer Hökelek, Mohamed Labd Taha, Joel T. Mague, Lhoussaine El Ghayati and El Mokhtar Essassi

Computing details

Data collection: *APEX3* (Bruker, 2016); cell refinement: *SAINT* (Bruker, 2016); data reduction: *SAINT* (Bruker, 2016); program(s) used to solve structure: *SHELXT* (Sheldrick, 2015*a*); program(s) used to refine structure: *SHELXL2018* (Sheldrick, 2015*b*); molecular graphics: *DIAMOND* (Brandenburg & Putz, 2012); software used to prepare material for publication: *SHELXTL* (Bruker, 2016).

(2*Z*)-4-Benzyl-2-(2,4-dichlorobenzylidene)-2*H*-1,4-benzothiazin-3(4*H*)-one

Crystal data

$C_{22}H_{15}Cl_2NOS$
$M_r = 412.31$
Monoclinic, $P2_1/c$
$a = 9.0373$ (7) Å
$b = 16.6798$ (13) Å
$c = 12.511$ (1) Å
$\beta = 95.982$ (2)°
$V = 1875.6$ (3) Å^3
$Z = 4$
$F(000) = 848$
$D_x = 1.460$ Mg m^{-3}
Cu $K\alpha$ radiation, $\lambda = 1.54178$ Å
Cell parameters from 9943 reflections
$\theta = 4.4$–43.5°
$\mu = 4.25$ mm^{-1}
$T = 150$ K
Block, colourless
0.14 × 0.13 × 0.09 mm

Data collection

Bruker D8 VENTURE PHOTON 100 CMOS diffractometer
Radiation source: INCOATEC IμS micro-focus source
Mirror monochromator
Detector resolution: 10.4167 pixels mm^{-1}
ω scans
Absorption correction: numerical (*SADABS*; Krause *et al.*, 2015)
$T_{min} = 0.59$, $T_{max} = 0.70$
48886 measured reflections
3847 independent reflections
3650 reflections with $I > 2\sigma(I)$
$R_{int} = 0.038$
$\theta_{max} = 74.6°$, $\theta_{min} = 4.4°$
$h = -11\rightarrow11$
$k = -20\rightarrow20$
$l = -15\rightarrow15$

Refinement

Refinement on F^2
Least-squares matrix: full
$R[F^2 > 2\sigma(F^2)] = 0.026$
$wR(F^2) = 0.070$
$S = 1.05$
3847 reflections
304 parameters
0 restraints
Secondary atom site location: difference Fourier map

Hydrogen site location: difference Fourier map
All H-atom parameters refined
$w = 1/[\sigma^2(F_o^2) + (0.0379P)^2 + 0.6937P]$
where $P = (F_o^2 + 2F_c^2)/3$

$(\Delta/\sigma)_{max} = 0.001$
$\Delta\rho_{max} = 0.22$ e Å^{-3}
$\Delta\rho_{min} = -0.26$ e Å^{-3}

Special details

Geometry. All esds (except the esd in the dihedral angle between two l.s. planes) are estimated using the full covariance matrix. The cell esds are taken into account individually in the estimation of esds in distances, angles and torsion angles; correlations between esds in cell parameters are only used when they are defined by crystal symmetry. An approximate (isotropic) treatment of cell esds is used for estimating esds involving l.s. planes.

Refinement. Refinement of F^2 against ALL reflections. The weighted R-factor wR and goodness of fit S are based on F^2, conventional R-factors R are based on F, with F set to zero for negative F^2. The threshold expression of $F^2 > 2\text{sigma}(F^2)$ is used only for calculating R-factors(gt) etc. and is not relevant to the choice of reflections for refinement. R-factors based on F^2 are statistically about twice as large as those based on F, and R- factors based on ALL data will be even larger.

Fractional atomic coordinates and isotropic or equivalent isotropic displacement parameters (Å²)

	x	*y*	*z*	U_{iso}*/U_{eq}
Cl1	0.32725 (3)	0.51603 (2)	0.51778 (3)	0.03318 (9)
Cl2	−0.08376 (4)	0.45362 (2)	0.78449 (3)	0.03443 (10)
S1	0.15102 (3)	0.21109 (2)	0.37534 (2)	0.02451 (9)
O1	0.29675 (11)	0.36735 (6)	0.18264 (8)	0.0318 (2)
N1	0.36671 (11)	0.23777 (6)	0.20360 (8)	0.0231 (2)
C1	0.29233 (13)	0.14621 (7)	0.34225 (10)	0.0235 (2)
C2	0.30706 (15)	0.07308 (8)	0.39669 (11)	0.0287 (3)
H2	0.2413 (19)	0.0621 (10)	0.4526 (14)	0.033 (4)*
C3	0.41257 (16)	0.01777 (8)	0.37140 (12)	0.0327 (3)
H3	0.4187 (18)	−0.0323 (10)	0.4058 (13)	0.030 (4)*
C4	0.50780 (16)	0.03719 (8)	0.29531 (13)	0.0330 (3)
H4	0.579 (2)	−0.0001 (12)	0.2780 (15)	0.042 (5)*
C5	0.49570 (15)	0.11045 (8)	0.24245 (11)	0.0285 (3)
H5	0.5655 (19)	0.1230 (11)	0.1921 (13)	0.035 (4)*
C6	0.38507 (13)	0.16533 (7)	0.26301 (10)	0.0233 (2)
C7	0.29726 (13)	0.30575 (7)	0.23567 (10)	0.0237 (2)
C8	0.22305 (13)	0.30312 (7)	0.33731 (10)	0.0223 (2)
C9	0.20587 (14)	0.37330 (7)	0.38765 (10)	0.0241 (2)
H9	0.2472 (18)	0.4183 (10)	0.3553 (13)	0.031 (4)*
C10	0.13615 (13)	0.38965 (7)	0.48567 (10)	0.0232 (2)
C11	0.18203 (13)	0.45583 (7)	0.55067 (10)	0.0239 (2)
C12	0.11763 (15)	0.47512 (8)	0.64272 (11)	0.0266 (3)
H12	0.152 (2)	0.5194 (11)	0.6845 (14)	0.040 (5)*
C13	0.00202 (14)	0.42783 (8)	0.67128 (10)	0.0261 (3)
C14	−0.04785 (15)	0.36229 (8)	0.61082 (11)	0.0283 (3)
H14	−0.130 (2)	0.3302 (11)	0.6306 (14)	0.038 (4)*
C15	0.01925 (15)	0.34384 (8)	0.51908 (11)	0.0271 (3)
H15	−0.019 (2)	0.3021 (11)	0.4758 (15)	0.042 (5)*
C16	0.43514 (15)	0.24544 (8)	0.10287 (10)	0.0261 (3)
H16A	0.4342 (18)	0.1915 (10)	0.0694 (13)	0.029 (4)*
H16B	0.3717 (18)	0.2771 (10)	0.0550 (13)	0.027 (4)*

C17	0.59004 (14)	0.28115 (7)	0.11411 (10)	0.0235 (2)
C18	0.65243 (16)	0.30239 (9)	0.02058 (11)	0.0311 (3)
H18	0.593 (2)	0.2943 (11)	−0.0487 (15)	0.039 (5)*
C19	0.79411 (17)	0.33523 (9)	0.02566 (13)	0.0384 (3)
H19	0.835 (2)	0.3503 (12)	−0.0383 (16)	0.050 (5)*
C20	0.87604 (17)	0.34739 (9)	0.12401 (14)	0.0382 (3)
H20	0.973 (2)	0.3695 (12)	0.1271 (15)	0.046 (5)*
C21	0.81497 (16)	0.32701 (8)	0.21707 (13)	0.0334 (3)
H21	0.874 (2)	0.3354 (11)	0.2875 (14)	0.040 (5)*
C22	0.67257 (15)	0.29448 (8)	0.21258 (11)	0.0273 (3)
H22	0.6283 (17)	0.2799 (9)	0.2793 (12)	0.024 (4)*

Atomic displacement parameters (Å²)

	U^{11}	U^{22}	U^{33}	U^{12}	U^{13}	U^{23}
Cl1	0.02604 (16)	0.03290 (17)	0.04160 (19)	−0.00735 (12)	0.00829 (13)	−0.00211 (13)
Cl2	0.03839 (18)	0.03495 (18)	0.03231 (17)	0.00967 (13)	0.01489 (13)	0.00164 (12)
S1	0.02266 (15)	0.02109 (15)	0.03075 (17)	−0.00207 (11)	0.00738 (12)	0.00098 (11)
O1	0.0405 (5)	0.0264 (5)	0.0303 (5)	0.0018 (4)	0.0116 (4)	0.0066 (4)
N1	0.0226 (5)	0.0248 (5)	0.0224 (5)	−0.0006 (4)	0.0050 (4)	0.0000 (4)
C1	0.0225 (6)	0.0217 (6)	0.0261 (6)	−0.0018 (5)	0.0009 (5)	−0.0017 (5)
C2	0.0297 (7)	0.0241 (6)	0.0321 (7)	−0.0029 (5)	0.0017 (5)	0.0022 (5)
C3	0.0349 (7)	0.0215 (6)	0.0406 (8)	0.0005 (5)	−0.0015 (6)	0.0025 (5)
C4	0.0295 (7)	0.0245 (6)	0.0446 (8)	0.0037 (5)	0.0022 (6)	−0.0047 (6)
C5	0.0253 (6)	0.0267 (6)	0.0337 (7)	−0.0007 (5)	0.0044 (5)	−0.0047 (5)
C6	0.0225 (6)	0.0214 (6)	0.0255 (6)	−0.0026 (5)	0.0004 (5)	−0.0020 (5)
C7	0.0223 (6)	0.0241 (6)	0.0247 (6)	−0.0015 (5)	0.0025 (5)	0.0010 (5)
C8	0.0194 (5)	0.0231 (6)	0.0246 (6)	0.0002 (4)	0.0034 (4)	0.0033 (4)
C9	0.0229 (6)	0.0224 (6)	0.0276 (6)	0.0000 (5)	0.0051 (5)	0.0036 (5)
C10	0.0228 (6)	0.0207 (6)	0.0265 (6)	0.0038 (5)	0.0041 (5)	0.0034 (4)
C11	0.0201 (6)	0.0224 (6)	0.0293 (6)	0.0025 (4)	0.0034 (5)	0.0033 (5)
C12	0.0259 (6)	0.0242 (6)	0.0293 (6)	0.0039 (5)	0.0015 (5)	−0.0006 (5)
C13	0.0265 (6)	0.0260 (6)	0.0267 (6)	0.0083 (5)	0.0069 (5)	0.0042 (5)
C14	0.0279 (6)	0.0238 (6)	0.0350 (7)	0.0014 (5)	0.0111 (5)	0.0048 (5)
C15	0.0281 (6)	0.0222 (6)	0.0318 (7)	−0.0001 (5)	0.0075 (5)	0.0002 (5)
C16	0.0273 (6)	0.0315 (7)	0.0196 (6)	−0.0010 (5)	0.0033 (5)	−0.0020 (5)
C17	0.0256 (6)	0.0215 (6)	0.0240 (6)	0.0032 (5)	0.0062 (5)	0.0002 (4)
C18	0.0344 (7)	0.0333 (7)	0.0271 (7)	0.0065 (6)	0.0104 (5)	0.0039 (5)
C19	0.0385 (8)	0.0330 (7)	0.0476 (9)	0.0061 (6)	0.0232 (7)	0.0101 (6)
C20	0.0270 (7)	0.0262 (7)	0.0630 (10)	−0.0002 (5)	0.0123 (6)	0.0026 (6)
C21	0.0290 (7)	0.0262 (7)	0.0442 (8)	−0.0002 (5)	−0.0002 (6)	−0.0042 (6)
C22	0.0294 (6)	0.0261 (6)	0.0265 (6)	−0.0009 (5)	0.0042 (5)	−0.0013 (5)

Geometric parameters (Å, º)

Cl1—C11	1.7357 (13)	C10—C11	1.4076 (18)
Cl2—C13	1.7382 (13)	C11—C12	1.3814 (18)
S1—C8	1.7525 (12)	C12—C13	1.3854 (19)

S1—C1	1.7561 (13)	C12—H12	0.940 (19)
O1—C7	1.2228 (16)	C13—C14	1.3781 (19)
N1—C7	1.3759 (16)	C14—C15	1.3874 (19)
N1—C6	1.4192 (16)	C14—H14	0.971 (19)
N1—C16	1.4661 (16)	C15—H15	0.928 (19)
C1—C2	1.3967 (18)	C16—C17	1.5143 (18)
C1—C6	1.4000 (18)	C16—H16A	0.993 (17)
C2—C3	1.387 (2)	C16—H16B	0.945 (16)
C2—H2	0.981 (18)	C17—C22	1.3899 (18)
C3—C4	1.387 (2)	C17—C18	1.3965 (18)
C3—H3	0.938 (17)	C18—C19	1.388 (2)
C4—C5	1.388 (2)	C18—H18	0.979 (18)
C4—H4	0.94 (2)	C19—C20	1.383 (2)
C5—C6	1.3990 (18)	C19—H19	0.95 (2)
C5—H5	0.960 (18)	C20—C21	1.382 (2)
C7—C8	1.4988 (17)	C20—H20	0.95 (2)
C8—C9	1.3458 (18)	C21—C22	1.392 (2)
C9—C10	1.4616 (17)	C21—H21	0.993 (18)
C9—H9	0.948 (17)	C22—H22	0.992 (16)
C10—C15	1.4024 (18)		

Cl1···Cl1^{i}	3.2439 (5)	C6···C22	3.4830 (18)
Cl1···C14^{ii}	3.4981 (14)	C6···C12^{v}	3.5828 (18)
Cl1···H9	2.647 (16)	C7···C22	3.4391 (18)
Cl2···H19^{iii}	2.96 (2)	C10···C12^{ii}	3.4871 (18)
Cl2···H9^{ii}	3.044 (16)	C14···C20^{iv}	3.572 (2)
Cl2···H4^{iv}	3.138 (18)	C5···H16A	2.563 (16)
S1···Cl2^{v}	3.5832 (5)	C6···H22	2.904 (15)
S1···Cl2^{v}	3.5832 (5)	C8···H15	2.929 (18)
S1···N1	3.0801 (11)	C16···H5	2.556 (18)
S1···C15	3.1625 (14)	C17···H5	2.829 (18)
S1···C13^{v}	3.6033 (13)	C18···H3^{vi}	2.998 (17)
S1···H15	2.578 (18)	C21···H12^{i}	2.845 (18)
O1···C17	3.2096 (16)	H14···C20^{iv}	2.964 (18)
O1···C4^{vi}	3.3346 (17)	H14···C21^{iv}	2.899 (18)
O1···H9	2.406 (16)	H14···C22^{iv}	2.990 (18)
O1···H16B	2.345 (16)	H15···C19^{iv}	2.951 (18)
O1···H4^{vi}	2.51 (2)	H16B···S1^{v}	2.852 (16)
N1···S1	3.0801 (11)	H16B···C1^{v}	2.973 (16)
N1···H22	2.552 (15)	H18···C6^{v}	2.934 (19)
C1···C12^{v}	3.4639 (18)	H5···H16A	2.16 (2)
C1···C13^{v}	3.4372 (18)	H12···H21^{i}	2.46 (3)
C2···C12^{v}	3.541 (2)	H15···H21^{viii}	2.51 (3)
C3···C3^{vii}	3.485 (2)	H16B···H18	2.51 (2)
C5···C22	3.4988 (19)	H18···H22^{v}	2.53 (2)
C5···C17	3.4201 (18)		

C8—S1—C1	100.14 (6)	C11—C12—C13	118.49 (12)

C7—N1—C6	125.51 (10)	C11—C12—H12	120.1 (11)
C7—N1—C16	115.14 (10)	C13—C12—H12	121.4 (11)
C6—N1—C16	119.20 (10)	C14—C13—C12	121.49 (12)
C2—C1—C6	120.71 (12)	C14—C13—Cl2	119.70 (10)
C2—C1—S1	117.26 (10)	C12—C13—Cl2	118.79 (10)
C6—C1—S1	122.02 (10)	C13—C14—C15	118.94 (12)
C3—C2—C1	120.17 (13)	C13—C14—H14	120.9 (10)
C3—C2—H2	121.4 (10)	C15—C14—H14	120.1 (10)
C1—C2—H2	118.5 (10)	C14—C15—C10	122.24 (12)
C4—C3—C2	119.47 (13)	C14—C15—H15	118.7 (12)
C4—C3—H3	120.7 (10)	C10—C15—H15	118.9 (12)
C2—C3—H3	119.8 (10)	N1—C16—C17	115.04 (10)
C3—C4—C5	120.59 (13)	N1—C16—H16A	107.3 (9)
C3—C4—H4	119.6 (12)	C17—C16—H16A	111.3 (9)
C5—C4—H4	119.7 (12)	N1—C16—H16B	108.1 (10)
C4—C5—C6	120.71 (13)	C17—C16—H16B	109.4 (10)
C4—C5—H5	118.7 (10)	H16A—C16—H16B	105.2 (13)
C6—C5—H5	120.6 (11)	C22—C17—C18	118.42 (12)
C5—C6—C1	118.24 (12)	C22—C17—C16	123.41 (11)
C5—C6—N1	120.50 (11)	C18—C17—C16	118.16 (12)
C1—C6—N1	121.26 (11)	C19—C18—C17	120.85 (14)
O1—C7—N1	120.68 (11)	C19—C18—H18	120.7 (11)
O1—C7—C8	120.54 (11)	C17—C18—H18	118.5 (11)
N1—C7—C8	118.78 (10)	C20—C19—C18	120.29 (14)
C9—C8—C7	117.09 (11)	C20—C19—H19	119.3 (12)
C9—C8—S1	124.79 (10)	C18—C19—H19	120.4 (12)
C7—C8—S1	117.88 (9)	C21—C20—C19	119.32 (14)
C8—C9—C10	129.48 (12)	C21—C20—H20	120.6 (11)
C8—C9—H9	114.8 (10)	C19—C20—H20	120.1 (11)
C10—C9—H9	115.7 (10)	C20—C21—C22	120.69 (14)
C15—C10—C11	116.15 (11)	C20—C21—H21	119.2 (11)
C15—C10—C9	123.53 (12)	C22—C21—H21	120.1 (11)
C11—C10—C9	120.29 (11)	C17—C22—C21	120.43 (13)
C12—C11—C10	122.68 (12)	C17—C22—H22	118.7 (9)
C12—C11—Cl1	117.23 (10)	C21—C22—H22	120.9 (9)
C10—C11—Cl1	120.08 (10)		

C8—S1—C1—C2	155.71 (10)	S1—C8—C9—C10	4.6 (2)
C8—S1—C1—C6	−25.73 (11)	C8—C9—C10—C15	−29.8 (2)
C6—C1—C2—C3	−1.12 (19)	C8—C9—C10—C11	152.34 (13)
S1—C1—C2—C3	177.47 (10)	C15—C10—C11—C12	0.42 (18)
C1—C2—C3—C4	3.0 (2)	C9—C10—C11—C12	178.46 (11)
C2—C3—C4—C5	−1.7 (2)	C15—C10—C11—Cl1	179.25 (9)
C3—C4—C5—C6	−1.5 (2)	C9—C10—C11—Cl1	−2.71 (16)
C4—C5—C6—C1	3.35 (19)	C10—C11—C12—C13	−0.78 (19)
C4—C5—C6—N1	−175.72 (12)	Cl1—C11—C12—C13	−179.64 (9)
C2—C1—C6—C5	−2.05 (18)	C11—C12—C13—C14	0.72 (19)
S1—C1—C6—C5	179.43 (9)	C11—C12—C13—Cl2	−177.88 (9)

C2—C1—C6—N1	177.02 (11)	C12—C13—C14—C15	−0.33 (19)
S1—C1—C6—N1	−1.50 (17)	Cl2—C13—C14—C15	178.27 (10)
C7—N1—C6—C5	−158.93 (12)	C13—C14—C15—C10	0.0 (2)
C16—N1—C6—C5	16.29 (17)	C11—C10—C15—C14	0.00 (19)
C7—N1—C6—C1	22.03 (18)	C9—C10—C15—C14	−177.97 (12)
C16—N1—C6—C1	−162.76 (11)	C7—N1—C16—C17	84.01 (14)
C6—N1—C7—O1	174.42 (12)	C6—N1—C16—C17	−91.69 (14)
C16—N1—C7—O1	−0.96 (17)	N1—C16—C17—C22	9.68 (18)
C6—N1—C7—C8	−5.15 (18)	N1—C16—C17—C18	−169.73 (11)
C16—N1—C7—C8	179.46 (10)	C22—C17—C18—C19	0.7 (2)
O1—C7—C8—C9	−23.67 (18)	C16—C17—C18—C19	−179.87 (13)
N1—C7—C8—C9	155.91 (11)	C17—C18—C19—C20	0.1 (2)
O1—C7—C8—S1	150.91 (10)	C18—C19—C20—C21	−0.4 (2)
N1—C7—C8—S1	−29.52 (15)	C19—C20—C21—C22	0.1 (2)
C1—S1—C8—C9	−145.73 (11)	C18—C17—C22—C21	−1.06 (19)
C1—S1—C8—C7	40.15 (10)	C16—C17—C22—C21	179.53 (12)
C7—C8—C9—C10	178.71 (12)	C20—C21—C22—C17	0.7 (2)

Symmetry codes: (i) −*x*+1, −*y*+1, −*z*+1; (ii) −*x*, −*y*+1, −*z*+1; (iii) *x*−1, *y*, *z*+1; (iv) *x*−1, −*y*+1/2, *z*+1/2; (v) *x*, −*y*+1/2, *z*−1/2; (vi) −*x*+1, *y*+1/2, −*z*+1/2; (vii) −*x*+1, −*y*, −*z*+1; (viii) *x*−1, *y*, *z*.

Hydrogen-bond geometry (Å, º)

D—H···*A*	*D*—H	H···*A*	*D*···*A*	*D*—H···*A*
C4—H4···O1^{ix}	0.936 (19)	2.51 (2)	3.3346 (17)	147.7 (15)
C16—H16*B*···S1^{v}	0.945 (16)	2.852 (16)	3.7011 (13)	149.9 (12)
C3—H3···*Cg*4^{ix}	0.938 (17)	2.901 (17)	3.6428 (15)	136.8 (13)
C14—H14···*Cg*4^{x}	0.971 (19)	2.710 (18)	3.5593 (15)	146.8 (14)
C18—H18···*Cg*1^{xi}	0.979 (18)	2.969 (18)	3.6759 (16)	130.0 (13)

Symmetry codes: (v) *x*, −*y*+1/2, *z*−1/2; (ix) −*x*+1, *y*−1/2, −*z*+1/2; (x) *x*−1, −*y*−1/2, *z*−1/2; (xi) *x*, −*y*−1/2, *z*−3/2.